Polarization resolved measurements with the new EUV Ellipsometer of PTB

Victor Soltwisch[a], Andreas Fischer[a], Christian Laubis[a], Christian Stadelhoff[a], Frank Scholze[a], and Albrecht Ullrich[b]

[a]Physikalisch-Technische Bundesanstalt, Abbestraße 2-12, 10587 Berlin

[b] Advanced Mask Technology Center, Rähnitzer Allee 9, 01109 Dresden, Germany

ABSTRACT

After having developed metrology with synchrotron radiation at the storage rings BESSY I and BESSY II for more than 25 years1, particularly also for the characterization of EUV optical components and detectors, PTB extended its capabilities for EUV metrology with respect to polarization resolved measurements, particularly in the spectral region around 13.5 nm. With the development of larger numerical aperture optics for EUV and advanced illumination concepts for lithographic imaging, the polarization performance of the optical elements becomes ever more important. At PTB, we use monochromatized bending magnet radiation for the characterization of the optical elements because of the superior temporal stability and rapid tuneability of the wavelength. Thus the polarization of the radiation is almost linear, depending on the vertical beamline acceptance angle, and cannot be manipulated. Therefore, we decided to equip the soft X-ray beamline which delivers particularly well collimated and highly linearly polarized radiation with a sample manipulator which allows freely setting the orientation of the plane of deflection. Thus we are able to characterize samples in any orientation with respect to the linear polarized direction. We additionally can add a linear polarization analyzer working with a rotatable Brewster reflector to analyze the state of polarization of the reflected beam.

We present first results on the polarization properties of EUV multilayer mirrors close to the Brewster angle where polarization selectivity up to several hundred is predicted from model calculations. We also present polarization resolved measurements of the EUV diffraction of absorber line patterns at EUV photomasks.

Keywords: EUV-reflectometry, EUV polarimetry

1. INTRODUCTION

By now, Extreme Ultraviolet Lithography2 (EUVL) has changed over from R&D to pilot production3, triggering development activities in numerous topics from sensor development4 to improvement of optical components5. This development is critically dependent on the availability of suitable metrology equipment6. To meet these requirements and based on about 30 years of experience7, the Physikalisch-Technische Bundesanstalt (PTB) operates an EUV metrology facility designed for at-wavelength metrology at electron storage ring BESSY II. A total uncertainty of 0.10 % for peak reflectance with a reproducibility of 0.05 % and a reproducibility of 1 pm for the center wavelength with an uncertainty in the center wavelength of 2 pm[8] 8 are achieved for measurements near normal incidence. Full-sized EUVL optics such as mirrors from the projection optics and collectors for EUV pulsed plasma sources, introduce two additional challenges for measurements: They are operated using unpolarized radiation and often at significantly higher angles of incidence (AOI) which we call oblique incidence9. For these higher AOI the angular alignment becomes more critical, compromising the achievable uncertainty of the center wavelength and the measured peak reflectance depends critically on the degree of polarization. A recent expansion of PTB’s EUV measurement facilities opened new options for polarization resolving instrumentation. A new beamline10 for the EUV wavelength range (5 nm to 50 nm) was set up at PTB's own electron storage ring 'Metrology Light Source' (MLS)11 in Berlin. The EUV-reflectometer 12 and detector calibration station13 are now operated at this beamline. The soft X-ray radiometry beamline at the storage ring BESSY II, which provides particularly well collimated and linearly polarized radiation 14 thus became available for the installation of a new instrument, an EUV ellipso-scatterometer15, which allows to orient the plane of reflection at an arbitrary direction with respect to the fixed incoming linear polarization.

We present first results on the polarization properties of EUV multilayer mirrors close to the Brewster angle where polarization selectivity up to 10^4 is predicted from model calculations. Using the combination of a highly polarized beam from the soft X-ray radiometry beamline and a polarizer for the detection, we could verify these predictions for actual

multilayer mirrors. We also present polarization resolved measurements of the EUV diffraction of absorber line patterns at EUV photomasks. Almost 10% difference in the first order diffraction efficiency of a line grating are observed. We compared in detail the polarization properties of two different EUV mask absorber stacks.

2. INSTRUMENTATION

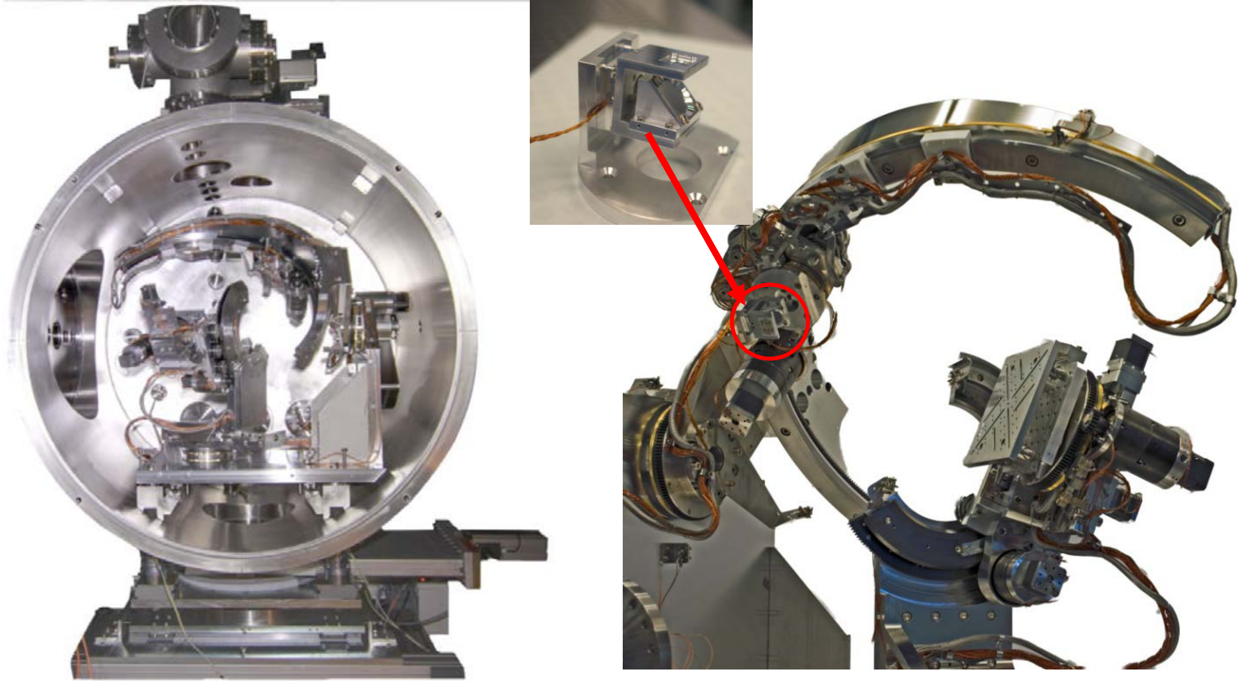

Figure 1: EUV Ellipso-Scatterometer of PTB. The sample stage can carry samples up to 190 mm square and 5 kg in mass. The mechanics are completely UHV compatible and lubrication free.

Figure 2 Detail of sample and detector stage of the EUV Ellipso-Scatterometer. The polarization analyzer at the detector stage is highlighted with a red circle. The inset shows the Brewster polarimeter in more detail. The rotary stage at the back and the mirror and diode mounting position on top are seen,

The data presented here were obtained at the soft X-ray radiometry beamline of PTB[16, 17]. It uses a plane grating monochromator which covers the spectral range from 0.7 nm to 35 nm and was especially designed to provide highly collimated radiation. It, therefore, uses a long focal length of 8 m in the monochromator, and the focusing in the non-dispersive direction is provided by the collecting pre-mirror with a focal length of 17 m. We achieve a collimation of the radiation in the experimental station better than 200 µrad and the scatter halo of the beam can be suppressed to below 10^{-5} relative intensity at an angle of only 1.7 mrad to the central beam[14]. The new ellipso-scatterometer of PTB [15], see Figure 1, is operated at this beamline. It allows rotating the plane of incidence (POI) around the axis of the incoming – linearly polarized – photon beam. This enables measurements in arbitrary polarization. For higher polarization selectivity a newly designed linear Brewster polarization analyzer was installed at the detector stage, see Figure 2. It is made up of a broad band EUV- multilayer mirror reflecting the incident beam under the Brewster angle onto a photodiode. The set-up can be rotated around the axis of the incident beam to define the plane of polarization. Using a set of three broad band Brewster mirrors we can cover the full spectral range which is potentially of interest for Mo/Si EUV mirrors from 12 nm to 15 nm.

3. EXPERIMENTS

3.1 Characterization of an EUV multilayer mirror close to the Brewster angle

To illustrate and verify the capabilities of the polarization analyzer, we measured the reflectance of a Mo/Si multilayer EUV-mirror close to the Brewster angle. Here, the reflectance for the P-polarized component, R_P, becomes very low values, according to model calculations using IMD as shown in Figure 3. Even the rather high degree of linear polarization of 98.7 %[14] is not sufficient to measure this because the remaining 0.65% P-polarized contribution in the

incoming beam are reflected by the mirror in the preferred S-polarization with the much higher reflectance for the P-polarized component, R_P, and mask completely the faint R_P reflectance component.

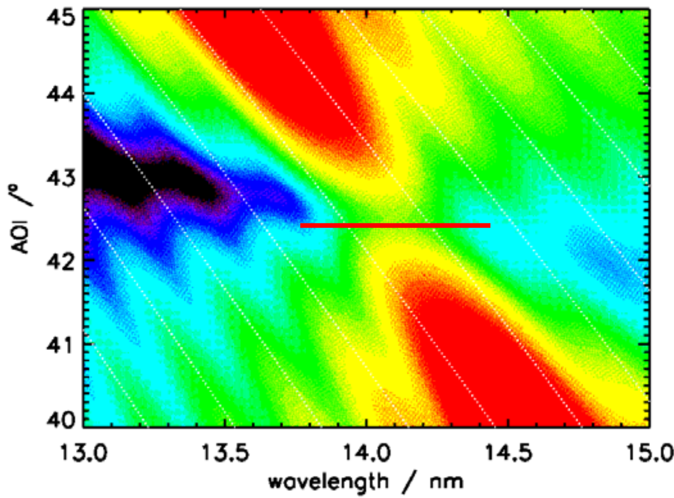

Figure 3 Calculated reflectance R_P of an Mo/Si multilayer mirror using model parameters adopted to measured reflectance for S-polarized radiation, R_S. The data are presented on a log. Intensity scale from $5{\cdot}10^{-6}$ (black) to 0.01 (red). The peak reflectance goes down to 10^{-3} at the Brewster angle of 42.5° (indicated by a red line). The dashed lines represent the shift of the center wavelength with AOI according to the Bragg equation for the multilayer, see also Figure 8.

Therefore, we used a Brewster analyzer in the reflected beam to suppress this component. To enable the wavelength tuning over the necessary spectral range with sufficient detection efficiency, the analyzer uses broad-band reflective coatings. With three exchangeable mirrors the analyzer supports measurements in the spectral range from 12 nm to 15 nm, see Figure 4. Figure 5 compares the reflectance R_S and R_P of the polarizer mirror. It shows a nice suppression ratio of better the 10^3 for the full spectral range covered by this mirror. Note that the range with high polarization selectivity is almost identical to the range of high S-polarized reflectance. It should also be noted that, for its own, this polarizer would not be sufficiently good the measure the suspected R_P of a standard multilayer mirror, which might be more than 10^4 times lower than R_S (see also Figure 7 below). Only the combination of a high degree of polarization from the beamline and the polarizer supports the high polarization selectivity needed.

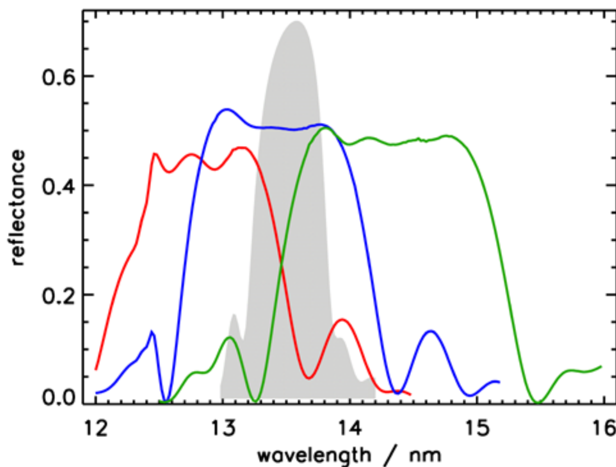

Figure 4 Reflectance of the analyzer mirrors at the working angle. The band pass of the middle mirror nicely covers the spectral of a standard 13.5-nm-EUV-mirror, shown as shadow in the back. The average reflectance of the analyzer mirrors is rather flat and around 50%.

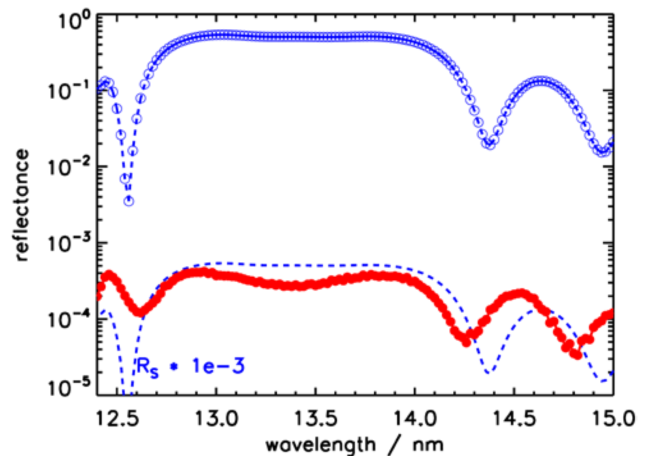

Figure 5 Reflectance for S- (blue open circles) and P-polarized (closed red circles) light for the analyzer mirror shown in blue in Figure 4. The S-reflectance is also shown downscaled by factor 1000 illustrating the P-polarization suppression ratio to be better than 1000 throughout the spectral range of the analyzer.

The polarization analyzer as shown here was used to measure the reflectance of a Mo/Si mirror close to the Brewster angle. The results are shown in Figure 6. With the polarizer we could analyze the S- and P-polarized components in the reflected radiation close to the Brewster angle with the mirror sample oriented in P-polarization reflection geometry. The

measured peak reflectance for the main S-polarized component (polarizer orientation "0°") of the incoming radiation goes down to 0.1 %, while the signal for the P-polarized component (polarizer orientation "90°")appears almost constant at around 0.4 % and shows also the characteristic much wider R_S – like reflectance curve. With about 65% reflectance for S-polarization, these 0.4 % correspond to a contribution of 0.62% P-polarized radiation in the incoming beam. This corresponds nicely to the above mentioned degree of 98.7 % linear polarization. The P-polarization reflectance is shown in Figure 7 in comparison to the S-polarization reflectance on a logarithmic scale together with model calculations using tabulated optical constants of Henke and a multilayer model fitted to the S-polarization reflectance. The P-polarization reflectance is in a reasonable but not perfect agreement.

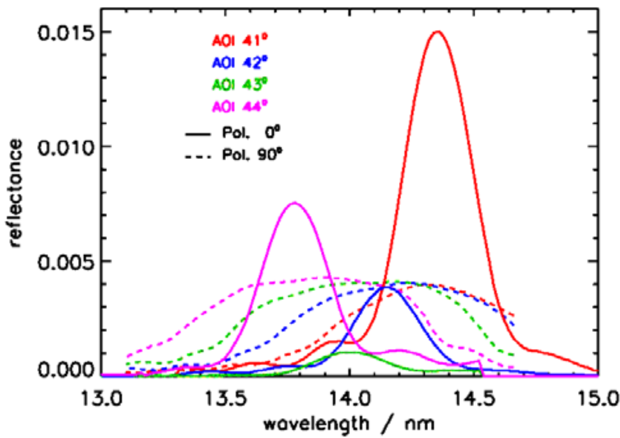

Figure 6 Reflectance of a Mo/Si mirror for different AOI close to the Brewster angle in P-polarization orientation. Data are shown for 2 orientations of the polarizer. The solid lines are data with polarizer transmitting S-polarized light while the dashed lines show the data with polarizer transmitting P-polarized light. Close to the Brewster angle (AOI 43°) the latter contribution is about 10 times higher.

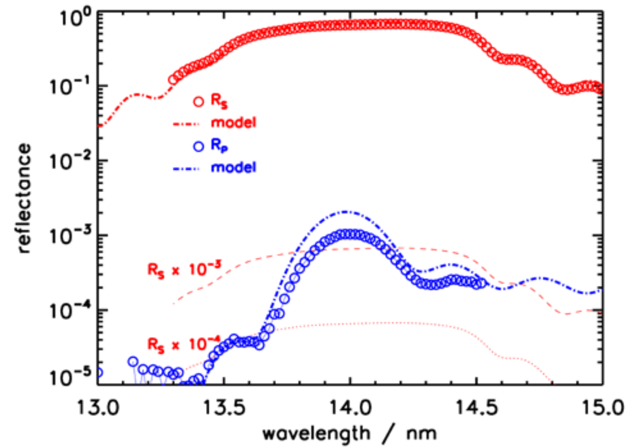

Figure 7 Comparison of the measured reflectance R_S and R_P of a Mo/Si mirror at the Brewster angle. The good suppression ratio of the polarization analyzer allows measuring R_P even in regions where it is more than 10^4 times lower than R_S. Also shown are some calculated curves for comparison

The discrepancy between the multilayer model and the measurement is shown in a different way below in Figure 8. Here, we compared the calculated reflectance R_P from Figure 3 shown as peak reflectance and center wavelength over AOI with the measured data. The peak reflectance shows the minimum at the Brewster angle while the center wavelength shows a wiggle in the cos-like dependence at this angle. Due to the narrow angular range the cos-like dependence from the Bragg equation appears almost linear in the plot, see also dashed trend lines Figure 3. Here it becomes clearer that the wiggle in the trend is causes by a phase shift of the reflected wave at the Brewster angle.

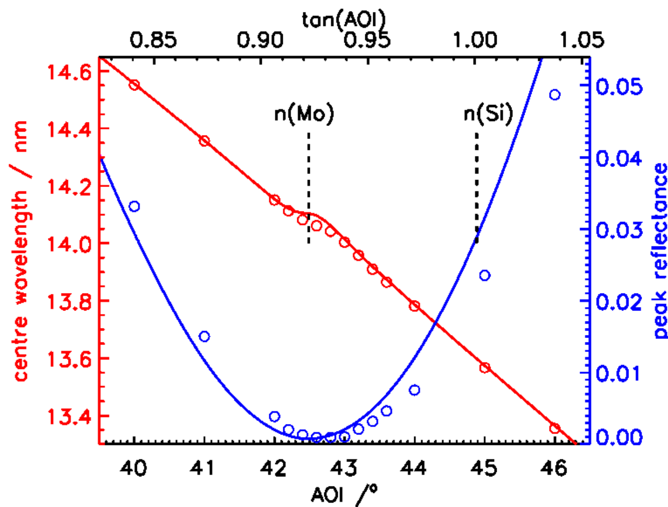

Figure 8 Comparison of the measured (blue circles) and modeled (blue line) reflectance R_P around the Brewster angle. Note the distinct kink in the modeled curve (red line) for the center wavelength at the position of the Brewster angle (minimum peak reflectance). The measured center wavelength is represented by the red open circles. The minimum peak reflectance as well as the kink in the center-wavelength-curve are shifted with respect to the calculation. The refractive indices of Mo and Si are indicated with respect to the upper scale.

The measured data follow the same trends with only the respective AOI slightly shifted to larger values. The Brewster angle is given by: $\tan(\Theta_B) = n_2 / n_1$ or, in our case, $n_1 = 1$ (vacuum) simply $\tan(\Theta_B) = n_2$. The upper scale in Figure 8 indicates $\tan(\Theta_B)$. The nominal refraction indices (Henke 18) for Si and Mo are shown in the graph with respect to this scale. It is obvious that the Brewster angle corresponds to the refractive index of Mo as the material with the lower value of n. It clearly not coincides with the average refractive index of a MoSi mixture. There is also no structure at the value of n for Si. It is worth noting that this measurement provides a direct access to the diffractive index of Mo as a buried layer in this system. Future investigations will be devoted to the exploration of the option for the measurement of optical constants without interference from surface oxidation or contamination which always compromises the straight forward approach of measuring reflectance versus AOI and fitting n&k from the Fresnel equations.

3.2 Polarization resolved EUV diffraction efficiency of absorber line structures at an EUV photomask

We measured the diffraction efficiency of dense line fields with representative CD values for current technology nodes. The structures were fabricated by AMTC at EUV substrates from two different suppliers which mainly differ in the absorber stack, particularly its thickness. The samples will be referred to as EUV#1 for the thinner absorber and EUV#2 for the thicker absorber. Studies on the EUV printing behavior of masks with different absorber thickness are already published back in 2011 [19]. The essential properties of the mask are given in this context by the diffraction efficiency into the different orders which are captured by the imaging lens of the litho machine. Here we present – to our knowledge – the first polarization resolved measurement of these diffraction efficiencies.

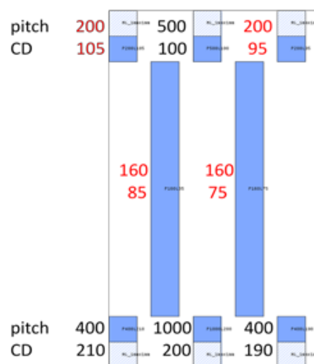

Figure 9 Layout of the scatter fields for metrology development at the EUV masks from AMTC. There are fields at similar pitch with biased CD to test for CD sensitivity as well as fields with semi-dense lines. The two large fields at 160 nm pitch are also suited for GISAXS.

This is illustrated below in Figure 10 and Figure 11. There are essentially two different orientations in the diffraction geometry, first the plane of the incident beam (POI) is parallel to the grating lines and the diffraction orders out of the POI, also referred to as "vertical lines" in mask pattern printing studies or the POI is perpendicular to the lines with the diffraction orders also in the POI; also referred to as "horizontal lines". For the case of vertical lines (Figure 10) there is

almost no difference for the TE and TM polarization direction. It is, however, remarkable that we observed a slight increase in the 0th order efficiency for TM polarization. This is in contrast to the usual behavior with the TM reflectance being lower than the TE reflectance. For the horizontal lines, the figure is different. Here we observe significantly reduced intensity in the 0th as well as $+1^{st}$ order. The -1st order is not affected. It should be noted these polarization effects are observed, although for EUV the structures at the mask level are much larger than the wavelength.

For the mask with the thicker absorber, EUV#2, these effects were studied in more detail. In Figure 12 and Figure 13 present wavelength scans at the respective -1st, 0th and $+1^{st}$ orders. The diffraction efficiencies for EUV#2 confirm the trends observed for EUV#1. For vertical lines, the values for TE and TM polarization are almost equal but again, the diffraction efficiency for the 0th order is slightly increased for TM polarization. For the horizontal lines the spectrally resolved measurements confirm the trends from EUV#1. Almost no polarization sensitivity for the -1st order and a significant reduction for the 0th and $+1^{st}$ order. Both trends hold for the full spectral range from 13 nm to 14 nm. Also the ratio of the TM diffraction efficiency with respect to the value for TE is equal for both masks being 0.955 for the 0th order and 0.915 for the 1st order.

Note that there is also a significant shift in the central wavelength between the -1st and $+1^{st}$ order. Particularly, the rather large shift of the -1st order to longer wavelengths cannot be attributed to the smaller enclosed angle between the incoming beam and the -1st order only. Due to the cos-behavior of the wavelength shift as given by Braggs equation, mostly the positive orders should be shifted to shorter wavelength because of the larger enclosed angle between the respective incident and diffracted beams. Such behavior must be taken into account when trying the balance the positive and negative diffraction orders for horizontal lines by tuning the multilayer reflectance towards longer wavelengths [20].

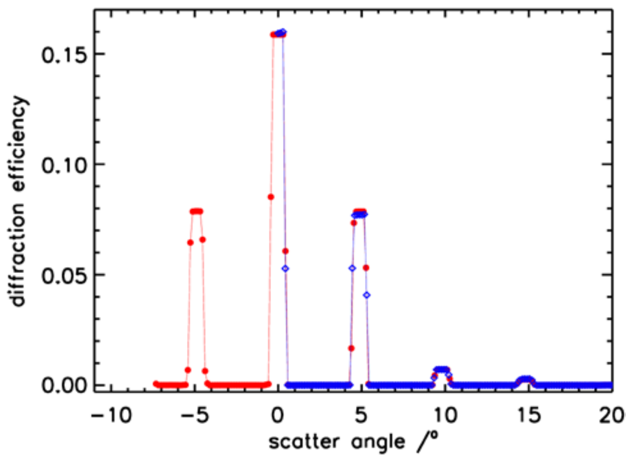

Figure 10 Diffraction efficiency of EUV#1 at 13.58 nm wavelength and AOI 6° to normal for vertical lines. Data are for TE (red dots) and TM (blue diamonds) polarization.

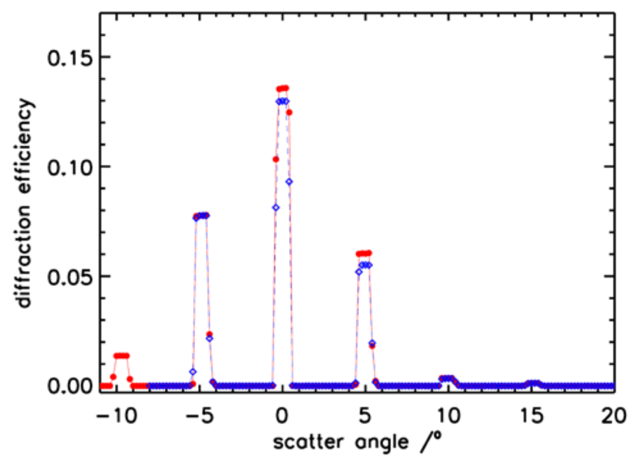

Figure 11 Diffraction efficiency as in Figure 10 for horizontal lines.

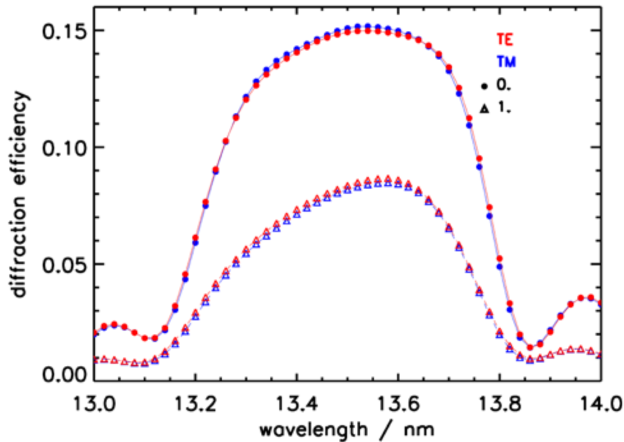

Figure 12 Diffraction efficiency of EUV#2 measured as function of wavelength for the 0th and 1st diffraction order at AOI 6° to normal with POI parallel to the grating lines (vertical lines). Due to the symmetry, the -1st and $+1^{st}$ order are equal. Red and blue represent the TE and TM polarization direction, respectively.

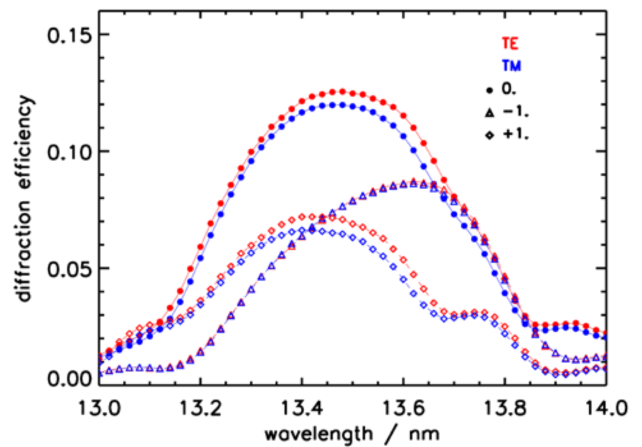

Figure 13 Diffraction efficiency of EUV#2 as in Figure 12. Here the POI is perpendicular to the grating lines (horizontal lines). Significant polarization effects are observed for the 0th und $+1^{st}$ order.

4. CONCLUSIONS

We demonstrated the feasibility to measure polarization dependent properties with a selectivity of better that 10^4. We could show evidence that such polarization sensitive measurements may provide an alternative way to investigate the optical properties of materials in buried layers. This offers the advantage that such layers are not exposed to oxidation or other disturbing effects. We also demonstrate the measurement of polarizing effects in the 0th and $\pm 1^{st}$ order diffraction at line structures on EUV photomasks. Although the representative pitches for present technology nodes are still more than 10x larger than the EUV wavelength, we could observe significant polarization effects at least for horizontal lines. As the EUV printing of horizontal lines is more critical due to the oblique incidence at the mask anyway, the full understanding and experimental verification of these effects is essential for the further optimization of EUV photomasks.

5. ACKNOWLEDGEMENT

References

[1] B.Beckhoff, et al.; Phys. Status Solidi B 246, 1415-1434 (2009)
[2] V. Bakshi, "EUV Lithography", John Wiley & Sons (2009)
[3] R. Peeters, ASML, talk "EUV Lithography: NXE3100 is in Use at Customer Sites and Building of NXE3300B has Started", Sematech EUVL Symposium, Miami (2011)
[4] L. Shi, S. Nihtianov, F. Scholze, A. Gottwald, L. Nanver, "High-sensitivity high-stability silicon photodiodes for DUV, VUV and EUV spectral ranges", Proc. SPIE **8145**, 81450N (2011)
[5] S. Yulin, IOF, talk "Reflective Optics for Next Generation Lithography", Sematech EUVL Symposium, Miami (2011)
[6] L. van Loyen et.al. "A new Laboratory EUV Reflectometer for Large Optics using a Laser Plasma Source", Proc. SPIE **5038**, 12-21 (2003)
[7] B. Beckhoff, A. Gottwald, R. Klein, M. Krumrey, R. Müller, M. Richter, F. Scholze, R. Thornagel, G. Ulm, "A quarter-century of metrology using synchrotron radiation by PTB in Berlin", Phys Status Solidii B, **246** 1415-1434 (2009)
[8] F. Scholze, C. Laubis, C. Buchholz, A. Fischer, S. Plöger, F. Scholz, H. Wagner and G. Ulm, "Status of EUV Reflectometry at PTB", Proc. SPIE **5751**, 749-758 (2005)

[9] C. Laubis, F. Scholze, C. Buchholz, A. Fischer, S. Hesse, A. Kampe, J. Puls, C. Stadelhoff and G. Ulm, " High accuracy EUV reflectometry at large optical components and oblique incidence", Proc. SPIE **7271**, 72713Y-1 (2009)

[10] C. Laubis, A. Fischer, F. Scholze, "Extension of PTB's EUV metrology facilities," Proc. SPIE: **8322**, 832236-1-9, (2012) dx.doi.org/10.1117/12.916414

[11] R. Klein, R. Thornagel, G. Ulm, J. Feikes, G. Wüstefeld, "Status of the Metrology Light Source", J. Electron Spectrosc. **184** (2011) 331-334

[12] J. Tümmler, G. Brandt, J. Eden, H. Scherr, F. Scholze, G. Ulm, "Characterization of the PTB EUV reflectometry facility for large EUVL optical components", Proc. SPIE **5037**, 265-273 (2003)

[13] F. Scholze, R. Klein, R. Müller, "Characterization of detectors for extreme UV radiation", Metrologia **43**, S6-S10 (2006)

[14] C. Laubis, A. Kampe, C. Buchholz, A. Fischer, J. Puls, C. Stadelhoff, F. Scholze, "Characterization of the polarization properties of PTB´s EUV reflectometry system," Proc. SPIE **7636**, 76362R (2010)

[15] F. Scholze, B. Bodermann, S. Burger, J. Endres, A. Haase, M. Krumrey, C. Laubis, V. Soltwisch, A. Ullrich, J. Wernecke; "Determination of line profiles on photomasks using DUV, EUV and X-ray scattering," Proc SPIE **9231** 92310M-1 - 92310M-11 (2014)

[16] R. Klein, C. Laubis, R. Müller, F. Scholze, G. Ulm, "The EUV metrology program of PTB," Microelectr. Eng. **83**, 707-709 (2006)

[17] F. Scholze, et al., "High-Accuracy EUV Metrology of PTB Using Synchrotron Radiation," Proc. SPIE **4344**, 402–413 (2001)

[18] B.L. Henke, E.M. Gullikson, and J.C. Davis. "X-ray interactions: photoabsorption, scattering, transmission, and reflection at E=50-30000 eV, Z=1-92," Atomic Data and Nuclear Data Tables Vol. 54 (no.2), 181-342 (July 1993)

[19] N. Davydova et al.; "Mask aspects of EUVL imaging at 27nm node and below," Proc. SPIE **8166** 816624-1 (2011)

[20] V. Philipsen, E. Hendrickx, E. Verduijn, S. Raghunathan, O. Wood, V. Soltwisch, F. Scholze, N. Davydova and P. Mangat, "Imaging impact of multilayer tuning in EUV masks, experimental validation," Proc SPIE **9235**, 92350J (2014)